Topological design of heat dissipating structure with forced convective heat transfer [†]

Gil Ho Yoon[*]

School of Mechanical Engineering, Kyungpook National University, Daegu, Korea

.

Abstract

This paper discusses the use of the topology optimization formulation for designing a heat dissipating structure that utilizes forced convective heat transfer. In addition to forced convection, there is also natural convection due to natural buoyancy forces induced by local heating inside fluid. In the present study, the temperature distribution due to forced convection, neglecting buoyancy and viscous dissipation inside fluid, was simulated and optimized. In order to analyze the heat transfer equation with forced convective heat loss and the Navier-Stokes equation, a common sequential computational procedure for this thermo/hydraulic characteristic was implemented. For topology optimization, four material properties were interpolated with respect to spatially defined density design variables: the inverse permeability in the Navier-Stokes equation, the conductivity, density, and the specific heat capacity of the heat transfer equation. From numerical examples, it was found that the balance between the conduction and convection of fluid is of central importance to the design of heat dissipating structures.

Keywords: Topology optimization; Forced convective heat transfer; Navier-Stokes equation; Heat transfer problem

---

1. Introduction

It remains a challenging task to efficiently analyze and design complex multiphysics systems coupled with more than two governing equations (see [1] for more details). Since the introduction of topology optimization theory, there has been much extensive research into applications of this innovative engineering design theory to the search for optimal multiphysics system structures [2-5]. The present study continued in that research vein in considering topological layout optimization to minimize thermal compliance, which is the product of temperature and heat input vectors [1]. The fluid motion and the heat transfer resulting from the forced convection induced by fluid motion were simultaneously analyzed, which is one of main contributions of the present research.

Convections typically are categorized, according to fluid motion origins, as *forced* or *natural* [6-9]. Natural convection, also called free or passive convection, involves a heat dissipating mechanism whereby temperature differences inside fluid initiates fluid motion through fluid density changes and induced buoyancy. Forced convection, contrastingly, entails heat dissipation where heat is carried passively by fluid motion initiated and maintained by external sources such as a fan

or a pump. These convections play important roles in various engineering applications such as electric devices [10-13] and food engineering [14-16].

From a computational point of view, multi-phase fluids with inhomogeneous densities and viscosities need to be implemented in order to analyze the natural convection model, which is much more complicated than the forced convection alternative. To our best knowledge, these difficulties associated with multi-phase fluids have yet to be researched further [8, 17]. Furthermore, because free convective flow velocities are usually much smaller than those associated with forced convection in most engineering applications, the corresponding convection heat rates are also much lower. Thus, only scant attention was paid to topology optimization for a heat dissipating structure limited to the forced convection model with simplified fluid motion; not considering the natural convection is one of the limitations of the present study.

Most of the existing research on topology optimization related to fluid has been geared towards finding an optimal distribution of the permeability or porosity of the fluid domain in order to optimize and control fluid flow [5, 18-22]. One of the novel ideas in the existing research are introducing the friction or damping force in the Navier-Stokes equation as an obstacle to the flow path and optimizing the friction coefficient, which determines porosities of subdomains, inside a design domain through topology optimization (see references [18-22] for detailed explanations of their advantages and drawbacks). In
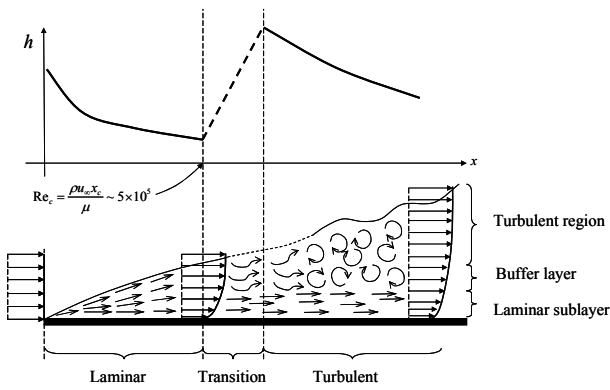
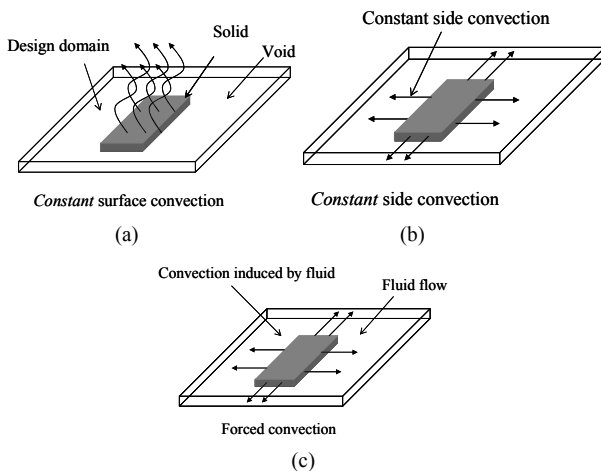Fig. 1. Fluid motion and convective coefficients [9].

Fig. 2. Convection models for topology optimization: (a) constant convection model; (b) constant side convection model; (c) forced convection model calculated by fluid motion.

other words, the velocities become almost zero at the subdomains assigned high friction coefficients, and can freely flow at subdomains having zero friction coefficients. To a certain extent, these computational approaches to topology optimization using the artificial friction force follow the same concept as the immersed boundary method (IBM) [17]. In addition, many topology optimization studies on the heat transfer problem have been conducted with the assumption of a constant *side* or *surface* convection coefficient, shown in Fig. 2(a, b) [1, 2, 23]. In our view, the problem here is that there is no research involving spatially varying convection considering the coupling between the Navier-Stokes equation and the heat transfer equation during topology optimization (Fig. 2(c)), which was investigated in the present study and is one of main contributions of this paper. To simplify topological optimization for the fluid and heat transfer interaction system, this study employed a common sequential analysis method neglecting buoyancy and viscous dissipation. Furthermore, following the approaches of [5, 18-22], the permeability of the Navier-Stoke's equation, the conductivity, the specific heat capacity, and the structural density of the heat transfer equation were interpolated with respect to spatially varying design
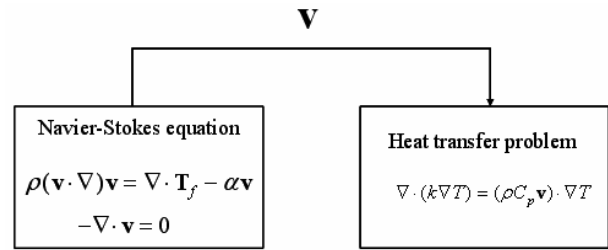

Fig. 3. Employed staggered analysis for thermo/hydraulic coupling system.

variables.

For successful topology optimization of the fluid-heat coupled multiphysics system, the present research assumed the following [8, 9]:

(a) an incompressible fully developed laminar fluid motion with a low Reynolds number (therefore, a deterministic rather than stochastic fluid motion)

(b) material properties of fluid that are independent of temperature

(c) viscous dissipating inside fluid was not accounted for in the energy balance equation.

First, only incompressible fully developed laminar fluid was considered, which is one of the limitations of this present research. As seen in Fig. 1, it is already a known fact that the convection coefficient of turbulent flow is larger than that of laminar flow. To analyze transient flow for averaged convection coefficients, it might be possible to employ a time-averaged analysis model such as the $k-\varepsilon$ fluid model [24], but such an exploration was not part of the present purposes. In any case, a full study of convection considering turbulent flow lies outside the scope of this investigation. Second, the material properties of the fluid were assumed to be independent of temperature. In reality, these velocities and temperatures are strongly coupled, and material properties of the coupled equations are dependent on each other [8, 9]. With the densities of flow varying with respect to temperature distribution, there can be, as already stated, fluid motions induced by buoyancy. For simplicity, these material dependences and other complexities stated above were neglected; however, this assumption is valid in many applications [10-16]. Finally, the scope was further restricted to the case where the viscous energy dissipation, a fluid-friction energy source [8, 9], was neglected.

The paper is organized as follows. After establishing the basic Navier-Stokes equation and the heat transfer equation coupled with fluid velocities in Section 2, the essential interpolation functions for the material properties, computational issues and implementation are described in Section 3. Also in Section 3, several numerical examples of topology optimization applied to two-dimensional fluid-heat transfer problems are presented. The final Section 4 summarizes the findings and identifies possible future research topics.
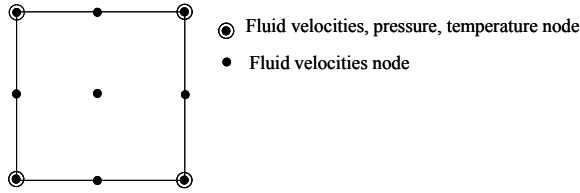
Fig. 4. Q2-P1 element satisfying inf-sup condition for coupled equations.

2. Coupled multiphysics analysis of fluid and heat transfer equation for topology optimization

To solve the underlying thermo/hydraulic problem, a staggered analysis approach in a unified domain, illustrated in Fig. 3, was taken. The velocities and pressure of the fluid domain were calculated from the Navier-Stokes equation and the velocities were, of necessity, inserted into the convective heat transfer equation to determine the temperature distribution. This immediate thermo/hydraulic problem does not require an explicit boundary between fluid and heat transfer domains, whereas other multiphysics systems require explicit boundaries among domains as simulated by each of the physics, which makes the application of existing analysis procedures for topology optimization numerically complex. Furthermore, it is not necessary to alternate the two governing equations in space according to the density design variables, which is one of important issues of topology optimization in other multiphysics systems. (This is too involved a subject to be treated in detail here. See [4, 5] for more in this issue.)

2.1 Analysis formulation for fluid and heat transfer problem

2.1.2 Navier-stokes equation

Fluid is treated as a continuum, mathematically implying that fluid can be identified as being at a specific point in space at one time with neighboring fluid while simultaneously at another specific point in space at a later time with the same neighbors. Thus the steady state Navier-Stokes equation and the incompressibility constraint with the substantive derivative are used as follows [8]:

Momentum: $\rho(\mathbf{v} \cdot \nabla)\mathbf{v} = \nabla \cdot \mathbf{T}_f - \alpha \mathbf{v}$ in Ω

(Ω : fluid domain) (1)

Continuity: $-\nabla \cdot \mathbf{v} = 0$ in Ω (2)

where the fluid velocity field and pressure of incompressible fully developed laminar flow are described by $\mathbf{v}$ and $p,$ respectively. The fluid density is denoted by ρ. The material derivative operator ∇ at the time t is defined at the control volume Ω. In Eq. (1), the friction force $\alpha \mathbf{v}$ is introduced for topology optimization, the concept of which shares a similarity with the immersed boundary method (IBM) (see [17] and references therein). Obviously, velocities become almost zero with a large α (α_{max}). Therefore, the following conditions can be devised.

$$\begin{cases} \alpha = \alpha_{max} \gg 0 \text{ for solid or non-fluid} \\ \alpha = 0 \text{ for fluid} \end{cases} \quad (3)$$

It could be possible to change or interpolate this coefficient at each point in a design domain to optimize flow channels.

The fluid symmetric stress $\mathbf{T}_f$ (i.e. the fluid stress) is given as Eq. (4),

$$\mathbf{T}_f = -p\mathbf{I} + \mu(\nabla \mathbf{v} + \nabla \mathbf{v}^\mathrm{T}) \quad (4a)$$

$$T_{f,ij} = -p\delta_{ij} + \mu(\frac{\partial v_i}{\partial x_j} + \frac{\partial v_j}{\partial x_i}) $$

(where $i, j = 1,2$ for 2D and $1,2,3$ for 3D) (4b)

where the viscosity having dimensions of stress-time is μ for Newtonian flow. Generally it is assumed that the fluid control volume, Ω, has the following boundary conditions.

Pressure boundary condition: $\mathbf{T}_f \cdot \mathbf{n} = p_p \cdot \mathbf{n}$ on Γ_{p^*} (5)

No slip boundary condition: $\mathbf{v} = \mathbf{0}$ on Γ_{v^0} (6)

Inflow/outflow boundary condition: $\mathbf{v} = \mathbf{v}^*$ on Γ_{v^*} (7)

The Dirichlet boundary conditions are imposed on Γ_{v^*} for a prescribed velocity ($\mathbf{v}^*$) and Γ_{v^0} for $\mathbf{v} = \mathbf{0}$, respectively. The Neumann boundary condition for the applied pressure p_p is defined at Γ_{p^*} with a normal vector $\mathbf{n}$.

2.1.3 The convective heat transfer equation

The general energy balance equation can be described as

Energy balance: $\dot{q} + \mu\Phi + \nabla \cdot (k\nabla T) = (\rho C_p \mathbf{v}) \cdot \nabla T$ in Ω

(8)

$$\mu\Phi = \mathbf{T}_f : \nabla \mathbf{v} \quad (9)$$

where the generated heat per volume and the viscous dissipation are denoted by $\dot{q}$ and $\mu\Phi$, respectively. The thermal conductivity and the specific heat capacity (thermal mass) of fluid are denoted by k and C_p, respectively. The viscous dissipation has the relationship of (9) with the fluid stress tensor and velocities, which is neglected in this study.

For simplicity, this research omitted this viscous dissipation term, $\mu\Phi$, from Eq. (8) and degenerated it into the following equation (although this computational model is expected to be reasonably accurate for most engineering applications [10-16], the issue of this viscous dissipation term can be considered to be important with a high viscosity, which itself is a full research topic within the realm of viscoelastic materials analysis):

$$\nabla \cdot (k\nabla T) = (\rho C_p \mathbf{v}) \cdot \nabla T \text{ in } \Omega \quad (10)$$

As the boundary conditions, the following heat input and adiabatic conditions were employed.

Adiabatic boundary condition: $(k\nabla T) \cdot \mathbf{n} = 0$ on Γ_A (11)

Heat input condition: $(k\nabla T) \cdot \mathbf{n} = q_{in}$ on $\Gamma_{q_{in}}$ (12)
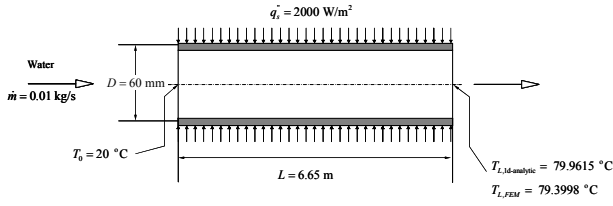
Fig. 5. Axisymmetric benchmark problem with analytical solution (Unscaled geometry).

Temperature condition: $T = T_{in}$ on Γ_T (13)

The Neumann boundary condition for the input heat q_{in} and the adiabatic condition are defined at $\Gamma_{q_{in}}$ and Γ_A respectively with a normal vector $\mathbf{n}$. The Dirichlet boundary condition is imposed at Γ_T.

2.2 Finite element formulation

To compute the solutions of Eqs. (10), (1), and (2), this study employed the finite element procedure from page 677 of [7] (see [7, 25] for examples of finite element implementation). For stabilized numerical analyses, Q2-P1 elements satisfying the inf-sup condition were employed (Fig. 4).

In general, the finite element formulation

$$(\mathbf{K}_{\mu vv} + \mathbf{K}_{vv} + \mathbf{K}_{alpha})\mathbf{V} + \mathbf{K}_{vp}\mathbf{P} = \mathbf{R}$$
$$\mathbf{K}_{vp}^T\mathbf{V} = \mathbf{0}$$ (14)

$$(\mathbf{K}_{vT} + \mathbf{K}_{TT})\mathbf{T} = \mathbf{Q}$$ (15)

can be derived, where $\mathbf{K}_{\mu vv}, \mathbf{K}_{vv}$, and $\mathbf{K}_{vp}$ are stiffness matrices of the Navier-Stoke equation and where $\mathbf{R}$ is the force matrix. The friction force matrix for $\alpha\mathbf{v}$ is $\mathbf{K}_{alpha}$. The heat input is $\mathbf{Q}$. The stiffness matrices of the heat equation are denoted by $\mathbf{K}_{vT}$ and $\mathbf{K}_{TT}$. The velocity, pressure and temperature vectors are $\mathbf{V}, \mathbf{P}$ and $\mathbf{T}$, respectively. (See page 677 in [7] for a more detailed implementation and equations for two-dimensional analysis. An MEX based on matlab can also be found in [25].) Because the above equations are nonlinear due to $\mathbf{K}_{vv}$ and $\mathbf{K}_{vT}$, the Newton-Raphson iteration

$$\Re(\mathbf{V}, \mathbf{P}, \mathbf{T}) = \begin{bmatrix} \mathbf{K}_{\mu vv} + \mathbf{K}_{vv} + \mathbf{K}_{alpha} & \mathbf{K}_{vp} & \mathbf{0} \\ \mathbf{K}_{vp}^T & \mathbf{0} & \mathbf{0} \\ \mathbf{0} & \mathbf{0} & \mathbf{K}_{vT} + \mathbf{K}_{TT} \end{bmatrix} \begin{bmatrix} \mathbf{V} \\ \mathbf{P} \\ \mathbf{T} \end{bmatrix} - \begin{bmatrix} \mathbf{R} \\ \mathbf{0} \\ \mathbf{Q} \end{bmatrix}$$ (16)

was employed to solve the equations iteratively, where the residual vector is denoted by $\Re(\mathbf{V}, \mathbf{P}, \mathbf{T})$. For numerical efficiency, the Navier-Stokes equations are solved before the heat equation, as shown in Fig. 3.

2.3 Heat transfer analysis for axisymmetric tube

In order to verify the developed numerical approach of Fig. 3, the computed solution of the axisymmetric heat transfer problem shown in Fig. 5 was compared with the one-

Table 1. Interpolated material properties in present approach.

	Heat transfer equation			Fluid equation
	K (Conductivity)	C_p (Specific heat capacity)	ρ (Density)	α (Friction coefficient)
Fixed domain ($\gamma = 1$)	k_s	C_s	ρ_s	$\alpha_{max} \gg 0$
Thermo/hydraulic domain ($\gamma = 0$)	k_f	$C_f (\ll C_s)$	ρ_f	0

dimensional analysis in [9]. With a fully developed laminar flow in a tube having the heat input in the middle of the tube, the input heat is dissipated. As shown, the calculated temperature agreed well with the target temperature, which validates the accuracy of the developed numerical code.

$$T_{L,1d-analytic} = T_0 + \frac{\pi D q_s^* L}{\dot{m} C_p} \approx 79.9615 \, C^o$$ (17a)

$\dot{m} = 0.01$ kg/s, $C_p = 4184$ J/kg·K, L=6.65 m, q_s''=2000 W/m^2, D=60 mm (17b)

3. Topology optimization formulation and examples

To minimize the damages or malfunctions of machines or electronic devices, it is important to control their maximum temperatures during operations. Therefore, designing effective heat dissipating structures to cool hot components of these devices through conduction and convection has been an important research topic in thermal and fluid mechanics. Nowadays, based on computational fluid dynamics (CFD), it is common to study the effects of parameterized structural models and optimized parameters in the framework of mathematical programming methods such as sequential linear programming (SLP), sequential quadratic programming (SQP), and the method of moving asymptotes (MMA) [26]. As detailed in this section, using the standard numerical procedures depicted in Fig. 3 and the method of moving asymptotes, the optimal topologies of heat dissipating structures were found.

3.1 Material interpolation function

To carry out topological optimization successfully, the material properties such as specific heat capacity, conductivity, density, and friction coefficients in Eqs. (1), (2) and (10) were interpolated with respect to the design variables (γ) defined at each element and listed in Table 1.

C_s and C_f are the specific heat capacities for solids and fluids, respectively. The specific heat capacity for fluids (C_f) is a much smaller value than that for solids (C_s). The thermal conductivity and density of solids are denoted by k_s and ρ_s, respectively, and those of fluids, by k_f and ρ_f. For simplicity and generality, the solid isotropic material with penalization (SIMP) approach was used to interpolate the variables as follows.

$$k(\gamma) = (k_s - k_f)\gamma^n + k_f$$ (18)

$$C_p(\boldsymbol{\gamma}) = (C_s - C_f)\boldsymbol{\gamma}^n + C_f \qquad (19)$$

$$\rho(\boldsymbol{\gamma}) = (\rho_s - \rho_f)\boldsymbol{\gamma}^n + \rho_f \qquad (20)$$

$$\alpha(\boldsymbol{\gamma}) = (\alpha_{\max} - 0)\boldsymbol{\gamma}^n + 0 \qquad (21)$$

For the penalization factor, 3 was used for *n* unless stated otherwise.

For a stable optimization, it is important to use an appropriate value for the maximum friction coefficient $\alpha_{\max}$. Solid domains with a sufficiently large value for $\alpha_{\max}$ do not allow water to pass through, while a too-high value can lead to a numerical singularity. Therefore, in order to determine an appropriate upper bound for $\alpha_{\max}$, some guidelines considering the Reynolds number and the Darcy number have been provided [5, 18-22]. In the present study, the guideline of Eq. (22) was considered with empirical numerical tests to choose proper values to make subdomains simulated for solid impervious.

$$\alpha_{\max} \sim \frac{\mu}{DaL_c^2} \qquad (22)$$

where the characteristic length and the Darcy number are L_c and Da, respectively.

3.2 Numerical examples

To show the potential of the developed approach, several numerical examples were considered. As an objective, this study considered the thermal compliance ϕ, which is defined as the product of the external heat input and temperature distribution of Eq. (23), and is similar to the structural compliance. By minimizing this objective with a constant heat input, the maximum temperature of a considered structure can be minimized.[1] Furthermore, this objective function has also been researched for topology optimization with a constant surface convection model [1, 2].

The optimization formulation with the thermal compliance ϕ and the mass constraint can be stated as

$$\text{Min } \phi = \int_{q_{in}} T \times q_{in} d\Gamma \qquad (23)$$

$$\text{s.t. } \int_{\Omega_d} \gamma dv \le V^0$$

where the design domain is denoted by Ω_d and the volume limit by V^0.

The adjoint variable method (AVM) was applied to calculate the sensitivity value with respect to the density design variables defined at each element. Considering the boundary condition, the objective function of Eq. (23) can be obtained as
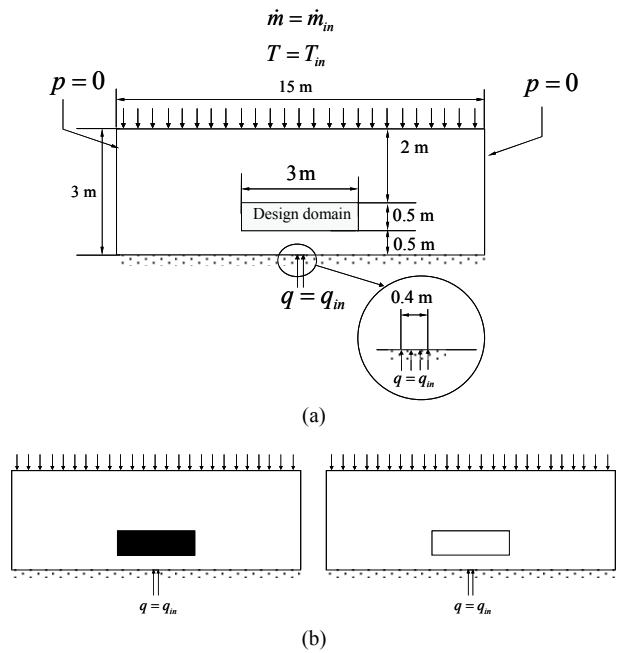

Fig. 6. Flow design problem over hot plate: (a) problem definition (Fluid: $\rho_{water} = 1000$ kg/m^3, $\eta_{water} = 1.308 \times 10^{-3}$ Pa·s, $k_{water} = 0.6$ W/m·K, $C_{water} = 4184$ J/kg·K, Solid (Copper): $\rho_s = 8920$ kg/m^3, $C_s = 385$ J/kg·K, $k_s = 401$ W/m·K, $\dot{m}_{in} = 0.15$ kg/s, $V_{in} = 1.0 \times 10^{-5}$ m/s, $T_{in} = 293$ K, $q_{in} = 100$ W/m^2, Reynolds number=114); (b) design tests of solid (Object = 1.3569×10^4 WK) and void (Object= 1.3196×10^4 WK).

$$\phi = \begin{bmatrix} 0 & 0 & \mathbf{Q}^T \end{bmatrix} \begin{bmatrix} \mathbf{V} \\ \mathbf{P} \\ \mathbf{T} \end{bmatrix} + \boldsymbol{\lambda}^T \cdot \boldsymbol{\Re} \qquad (24)$$

where the force vector and the Lagrange multiplier vector are denoted by $\mathbf{Q}$ and $\boldsymbol{\lambda}$, respectively. By differentiating the above equation, the following sensitivity analysis can be derived:

$$\phi' = \begin{bmatrix} 0 & 0 & \mathbf{Q}^T \end{bmatrix} \begin{bmatrix} \mathbf{V} \\ \mathbf{P} \\ \mathbf{T} \end{bmatrix}' + \boldsymbol{\lambda}^T (\frac{\partial \boldsymbol{\Re}}{\partial \gamma} + \frac{\partial \boldsymbol{\Re}}{\partial \begin{bmatrix} \mathbf{V} & \mathbf{P} & \mathbf{T} \end{bmatrix}} \begin{bmatrix} \mathbf{V} \\ \mathbf{P} \\ \mathbf{T} \end{bmatrix}')$$

$$(\text{where } ( )' = \frac{\partial ( )}{\partial \gamma}) \qquad (25)$$

$$\frac{\partial \phi}{\partial \gamma} = \boldsymbol{\lambda}^T \frac{\partial \boldsymbol{\Re}}{\partial \gamma} \text{ and } \boldsymbol{\lambda}^T \frac{\partial \boldsymbol{\Re}}{\partial \begin{bmatrix} \mathbf{V} & \mathbf{P} & \mathbf{T} \end{bmatrix}} = \begin{bmatrix} 0 & 0 & -\mathbf{Q}^T \end{bmatrix} \qquad (26)$$

After implementing the above sensitivity analysis, the accuracy of the calculated values were confirmed with the finite difference method (FDM).

3.2.1 Example 1: Minimizing thermal compliance

For the first example, the following design domain having a downward flow at the upper line and containing the boundary line having the heat input q_{in} was modeled, as shown in Fig. 6. The design variables determining the porosity, the conduction, and the convection could be distributed at the small rec-
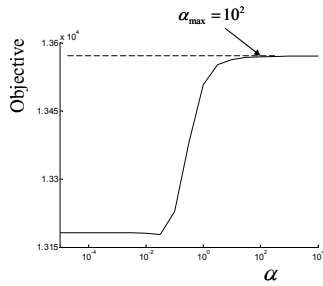
Fig. 7. Relationship of thermal compliance versus maximum alphas.
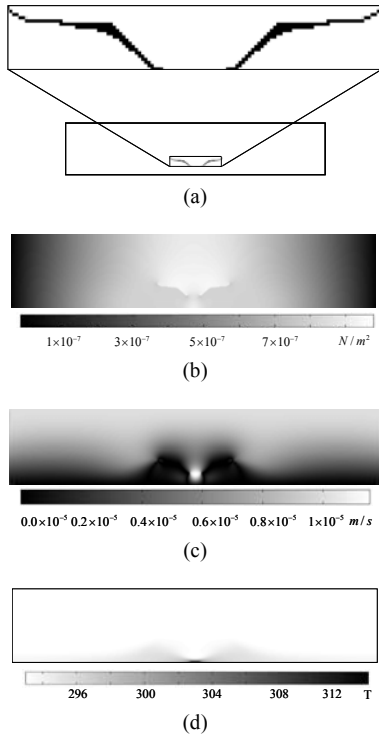

(a)

(b)

(c)

(d)

Fig. 8. Optimal layout with void initial guess: (a) density distribution (Object=1.2498×10^4 WK); (b) pressure; (c) absolute of vertical velocity; (d) temperature distribution.

tangular design domain positioned in the middle of the analysis domain. Before solving the optimization problem, it was not clearly understood whether the mass constraint in Eq. (23) was necessary or not; it was not a debatable point to use more material up to a given limit mass to make the compliant structure stiffer, but it was questionable whether more material makes a design efficient in terms of the heat dissipation. Thus, the thermal compliances of only the solid and void domains, which latter was filled with fluid, are compared in Fig. 6. The computed objective values of the void and solid designs indicates that less material is preferable in this specific optimization problem, which is opposite to the structural compliance minimization problem. From a physical point of view, this phenomenon is due to the fact that the solid box blocks the downward fluid motion and the solid design becomes inefficient in terms of the heat dissipation, even if any doubt remains about whether the thermal compliances increase or
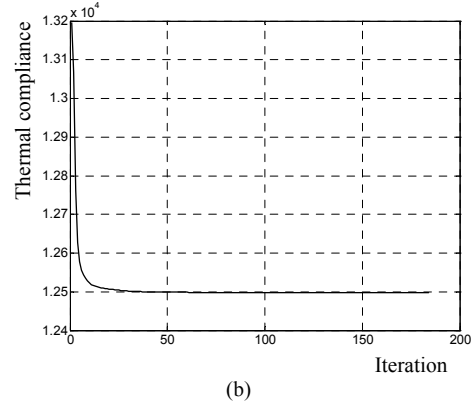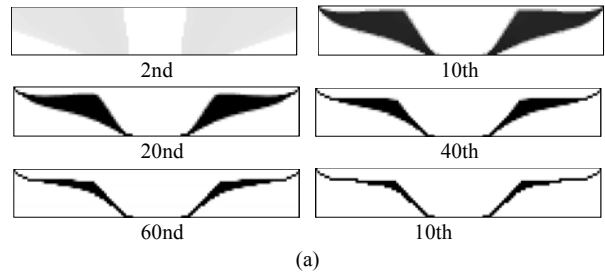

(a)

(b)

Fig. 9. Optimization histories: (a) intermediate designs; (b) object history.

decrease monotonically with respect to the mass usage percentage. Consequently, an attempt was made to solve the optimization without the mass constraint in this typical case. In addition, as stated in Subsection 3.1, it is important to use a proper maximum value for the inverse permeability, and so various upper values were empirically tested (Fig. 7), showing the convergence of the objective function. Because it was found that a real value over 100 is sufficient to make the domain impervious, that value was used for α_{max}. Fig. 8(a) shows an optimal design, along with the void initial density distribution and the pressure and velocities of the design. As shown, the optimized structure, whose mass usage is around 7.62%, collects the downward fluid in order to maximize the fluid velocity at the center and to minimize the thermal compliance. The Reynolds number of the considered problem was around 114, which satisfies the laminar flow condition. From several numerical tests varying the velocity of fluid and the characteristic length while maintaining the range of the Reynolds number, similar geometries could be found. The intermediate designs and the objective history are given in Fig. 9.

3.2.2 Example 2: Minimizing thermal compliance

For the second example, the design domain was changed, in Fig. 10, but the boundary condition and the material properties of the first example were retained. Unlike the first example, the design domain made a junction with the small solid box, which was filled with solid and which had the heat input q_{in}. To understand the effects of the design domain changes on the mass constraint, the objective values of the void and solid designs were calculated and compared. Again, unlike the first example, the objective value of the solid design was better
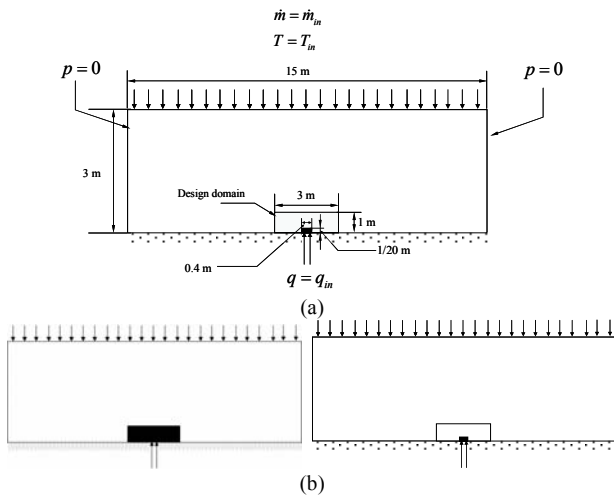
(a)

(b)

(c)

(d)

Fig. 12. Different local optima with various initial guesses: (a) local optima with 0.1 initial guess (Object= 1.1924×10^3 WK); (b) local optima with 0.3 initial guess (Object= 1.1895×10^3 WK); (c) local optima with 0.5 initial guess (Object= 1.1894×10^3 WK); (d) objective histories.

Fig. 10. Flow design problem over hot plate with unity thickness: (a) problem definition (Fluid: $\rho_{water} = 1000 \, kg/m^3$, $\eta_{water} = 1.308 \times 10^{-3}$ Pa·s, $k_{water} = 0.6 \, W/m \cdot K$, $C_{water} = 4184 \, J/kg \cdot K$, Solid (Copper): $\rho_s = 8920 \, kg/m^3$, $C_s = 385 \, J/kg \cdot K$, $k_s = 401 \, W/m \cdot K$, $\dot{m}_{in} = 0.15 \, kg/s$, $T_{in} = 293$ K, $q_{in} = 100 \, W/m^2$); (b) empirical design tests of solid (object $= 1.1907 \times 10^3$ WK) and void (object= 1.2946×10^4 WK).
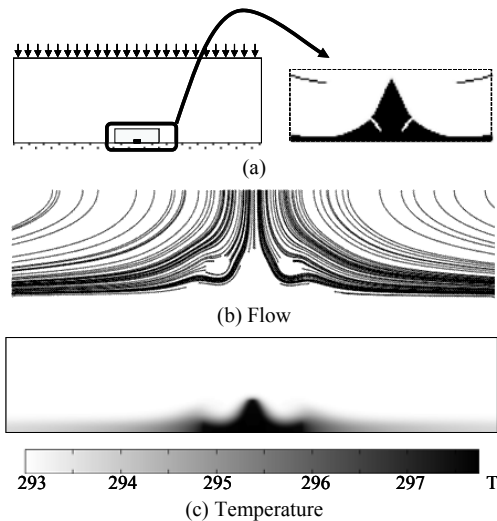

(a)

(b) Flow

(c) Temperature

Fig. 11. Optimized result (Object $= 1.1909 \times 10^3$ WK) with void initial guess (without the mass constraint, the black box (Object $= 1.1907 \times 10^3$ WK) is obtained).

than that of the void design, which might have been due to the fact that the convection surfaces became wider by filling the design domain. So in this example, the solid box might be the best design. Thus, the volume was constrained to 30% of the design domain here; the obtained design is shown in Fig. 11. From a physical point of view, the two side structures emerge to collect the downward flow and thereby maximize the convective heat transfer rates. Because the convective heat transfer rate is approximately proportional to the convection coefficient, flow velocity, and temperature difference, it is likely that topology optimization finds a local optimum that maximizes them simultaneously.
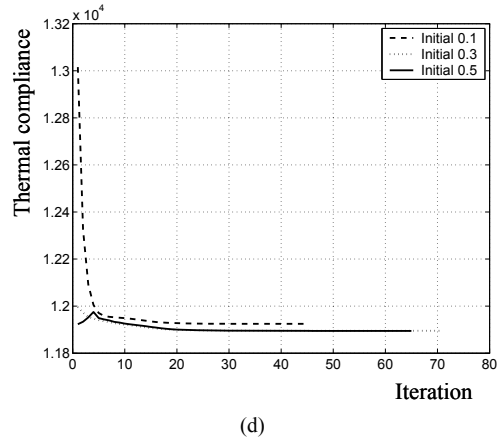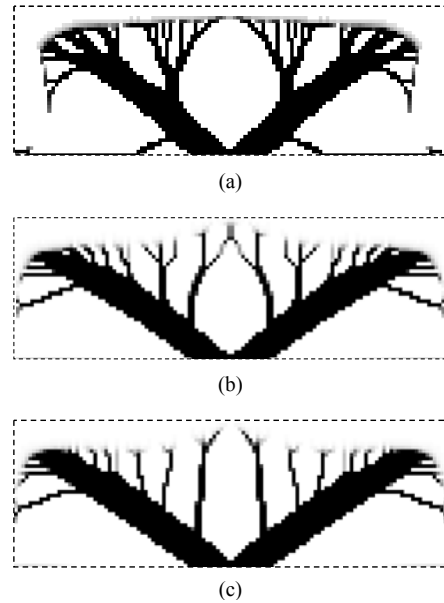
3.2.3 Local optima issue

Because a nonlinear multiphysics system was considered in this study, numerical difficulties such as many local optima and instabilities on the mesh-scale were observed. Thus, the present designs are definitely not global optima. To illustrate the local optima issue, Fig. 12 shows several different designs obtained with various initial guesses for the problem of Fig. 10. Because the heat loss from the convection is proportional to the fluid velocity and convection surfaces, it is likely that wider surface and complex shaped fin designs would be obtained. Note that the objective value of the design with the 0.5 initial guess is better than that of the design of Fig. 11 with the void initial guess.

3.2.4 Example 3: Minimizing thermal compliance by controlling fluid motion

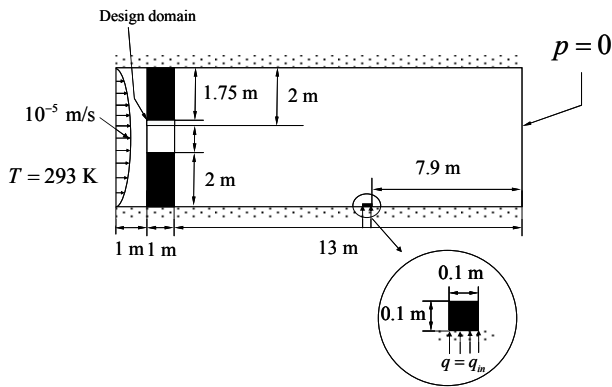As another numerical example, the design of an upper plate

Fig. 13. Flow design problem over hot plate: (a) problem definition (Fluid: $\rho_{water} = 1000$ kg/m³, $\eta_{water} = 0.352 \times 10^{-3}$ Pa·s, $k_{water} = 0.6$ W/m·K, $C_{water} = 4184$ J/kg·K, Solid(Copper): $\rho_s = 8920$ kg/m³, $C_s = 385$ J/kg·K, $k_s = 401$ W/m·K, $T_{in} = 293$ K, $q_{in} = 1 \times 10^4$ W/m²).
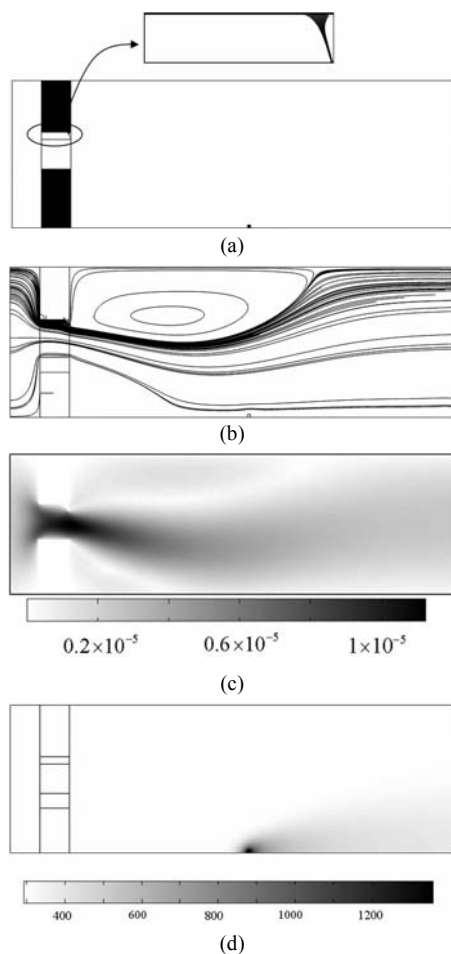

Fig. 14. Optimized result (Object = 135.9853 WK) with void initial guess: (a) density distribution; (b) flow lines; (c) fluid velocity; (d) temperature distribution.

inside the tube of Fig. 13 was considered. The objective of this problem is distributing materials to the part of the upper plate in order to minimize the thermal compliance of a box with a remote heat source. Fig. 14 shows the obtained design along with the flow lines and temperature. As shown, a slender

structure was obtained to change the flow toward the box with the heat input. This example also shows the potential usage of the present optimization method for design of a heat dissipation mechanism.

4. Conclusions

This paper concerns topology optimizations for a thermo/hydraulic heat dissipating system that utilizes forced convection. In considering this coupling system, the Navier-Stokes equation and the heat transfer equation were solved using the staggered analysis method depicted in Fig. 3. For simplicity, the material nonlinearities of the viscosity, the conductivity and the specific heat capacity were ignored, along with the viscous dissipation. In the Navier-Stokes equation, the artificial damping force, the concept of which is similar to that of the immersed boundary method (IBM), was included to simulate rigid boundaries, and its corresponding coefficient was interpolated from a very small number to a large number for topology optimization. In the heat transfer equation, the three associated material properties, which are the specific heat capacity, the density and the conductivity, were interpolated from those of fluids to those of solids for topology optimization. For the interpolation functions, the SIMP (Solid Isotropic Material with Penalization) was used to minimize thermal compliance due to input heat.

The potential of the present approach was demonstrated in the solution of three design problems. In these examples, it was found that, depending on design domains, there are some situations in which a solid box is not the best design, which is opposite to the structural compliance problem. From the numerical results, it was also found that the present approach can be used to design a forced convection heat dissipating structure. In a future study, turbulent flow will be considered so as to make the obtained results more realistic.

Acknowledgement

References

[1] M. P. Bendsøe and O. Sigmund, *Topology Optimization Theory, Methods and Applications*, Springer-Verlag, (2003).

[2] G. H, Yoon and Y. Y. Kim, The element connectivity parameterization formulation for the topology design optimization of multiphysics systems, *International Journal for Numerical Methods in Engineering*, 64 (2005) 1649-1677.

[3] G. H. Yoon, J. S. Jensen and O. Sigmund, Topology Optimization of Acoustic-Structure Interaction Problems using a

Mixed Finite Element Formulation, *International Journal for Numerical Methods in Engineering,* 70 (2007) 1049-1076.

[4] G. H. Yoon and O. Sigmund, A monolithic approach for electrostatic problems, *Computer Methods in Applied Mechanics and Engineering,* 197 (45-48) (2008) 4062-4075.

[5] G. H. Yoon, Topology optimization for stationary fluid–structure interaction problems using a new monolithic formulation, International journal for numerical methods in engineering, 82 (2010) 591-616.

[6] R. D. Cook, D. S. Malkus, M. E. Plesha and R. J. Witt, *Concepts and applications of finite element analysis.* John Wiley & Sons, USA, 4th Edition, (2001).

[7] K. J. Bathe, *Finite element procedures.* Prentice hall, New Jersey, (1996).

[8] Frank M. White, *Fluid Mechanics*, McGraw Hill International Edition, (1994).

[9] P. I. Frank, P. E. W. David, *Introduction to heat transfer*, Wiley, (1990).

[10] S. C. Lin, F. S. Chuang and C. A. Chou, Experimental study of the heat sink assembly with oblique straight fins, *Exp. Therm. Fluid Sci,* 29 (2005) 591-600.

[11] X. Yu, J. Feng, Q. Feng and Q. Weng, Development of a plate-pin fin heat sink and its performance comparisons with a plate fin heat sink, *Appl. Therm. Eng.,* 25 (2005) 173-182.

[12] M. A. Ismail, M. Z. Abdullah and M. A. Mujeebu, A CFD-based experimental analysis on the effect of free stream cooling on the performance of micro processor heat sinks, *International Communications in Heat and Mass Transfer,* 35 (2008) 771-778.

[13] S. C. Lin and C. L. Huang, An integrated experimental and numerical study of forward–curved centrifugal fan, *Experimental Thermal and Fluid Science,* 26 (2002) 421-434.

[14] M. V. D Bonis and G. Ruocco, A generalized conjugate model for forced convection drying based on an evaporative kinetics, *Journal of Food Engineering,* 89 (2008) 232-240.

[15] P. Verboven, N. Scheerlinck, J. D. Baerdemaeker and B. M. Nicolaï, Computational fluid dynamics modelling and validation of the isothermal airflow in a forced convection oven, *Journal of Food Engineering,* 43 (1) (2000) 41-53.

[16] C. Xu and T. S. Zhao, A new flow field design for polymer electrolyte-based fuel cells, *Electrochemistry Communications,* 9 (2007) 497-503.

[17] H. Luca, On the stability of the finite element immersed boundary method, *Computer and structures,* 86 (2008) 598-617.

[18] O. Fridolin and B. Henrik, Design of microfluidic bioreactors using topology optimization, European conference on computational fluid dynamics, ECCOMAS CFD 2006 Netherlands.

[19] T. Borrvall and J. Petersson, Topology optimization of fluids in stokes flow, *International Journal for Numerical Methods in Fluids,* 42 (2003) 77-107.

[20] J. K. Guest and J. H. Prevost, Topology optimization of creeping fluid flows using a Darcy–Stokes finite element, *International Journal for Numerical Methods in Fluids,* 66 (2006) 461-484.

[21] A. Gersborg-Hansen, O. Sigmund and R. B. Harber, Topology optimization of channel flow-problems, *Structural and Multidisciplinary Optimization,* 39 (3) (2005) 181-192.

[22] L. H. Olesen, F. Okkels and H. Bruus, A high-level programming-language implementation of topology optimization applied to steady-state Navier-Stokes flow, *International Journal for Numerical Methods in Engineering,* 65 (7*)* (2006) 975-1001.

[23] T. E. Bruns, Topology optimization of convection-dominated, steady-state heat transfer problems, *Int. J. Heat and Mass Transfer,* 50 (2007) 2859-2873.

[24] W. Xiaodong, Analytical and computational approaches for some fluid-structure interaction analyses, *Computer and structures,* 72 (1999) 423-433.

[25] P. O. Persson, Implementation of finite element-based navier-stokes solver, *http://persson.berkeley.edu/pub/nsfem_report. pdf,* (2002).

[26] K. Svanberg, The method of moving asymptotes - a new method for structural optimization, *International Journal for Numerical Methods in Engineering,* 24 (1987) 359-373.

Gil Ho Yoon is currently an Assistant professor at the mechanical department at the Kyungpook National University, Daegu, Korea. He focuses on structural optimization, multiphysics system, and nonlinear structures where he concentrates on optimization. He received a Ph.D. in school of mechanical and aerospace engineering from the Seoul National University in 2004, an MSc in 2000 and a BSc in 1998 from the same department and the same university.